Lázaro-Diéguez et al., http://www.jcb.org/cgi/content/full/jcb.201303013/DC1

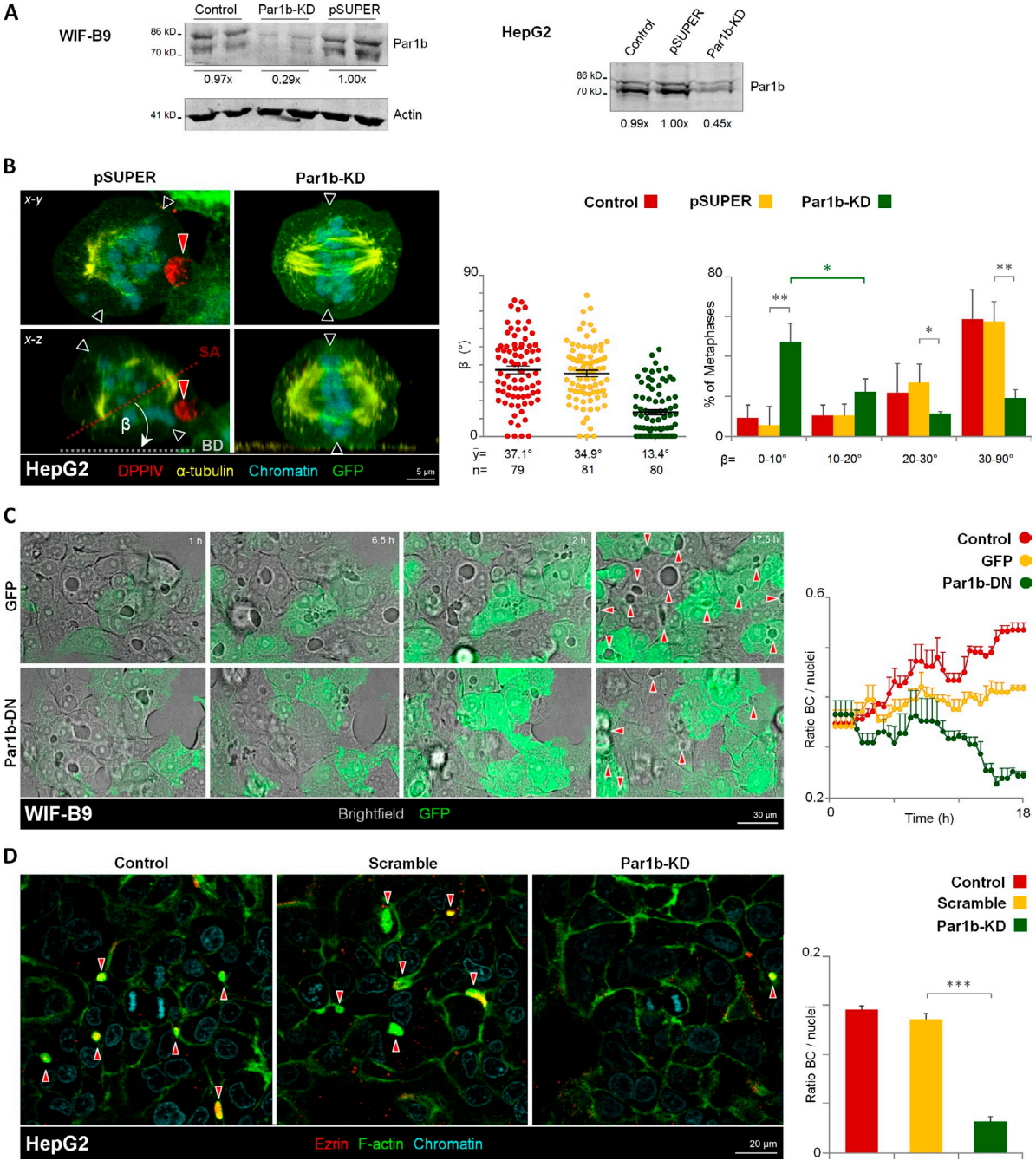

Figure S1. **Par1b depletion in WIF-B9 and HepG2 cells inhibits lateral lumen polarity and promotes spindle alignment with the basal domain.** (A) Par1b levels in WIF-B9 (left) and HepG2 (right) in untransduced cells (Control) or cells transduced with adenoviruses expressing a shRNA-Par1b construct (Par1-KD) and the corresponding control (pSUPER) empty vector. The double band corresponds to two Par1b splice variants. (B) Control and pSUPER-GFP or Par1b KD-GFP–expressing HepG2 cells were fixed and stained for DPPIV, α-tubulin, and chromatin, and the β angle was quantified. The percentage of Par1b-KD cells with a β angle in the 0–10° category (44.5 ± 9.5%) was higher than that in the 10–20° category (21.4 ± 7.9%) with statistical significance, indicating increased spindle alignment with the substratum by Par1b depletion. (C) Time-lapse sequence in untransduced WIF-B9 cells (Control) and cells transduced with adenoviruses expressing either GFP-tagged dominant-negative Par1b (Par1b-DN) or the corresponding control GFP protein. The amount of BC-like lumina was quantified (right). Error bars indicate ± SD of three experiments. (D) Control HepG2 cells and cells transiently transfected with Par1b siRNA or a control scrambled siRNA. Cells were fixed and stained for the apical protein ezrin, F-actin (phalloidin-TRITC), and chromatin. The amount of BC-like lumina in interphase cells (C, right) was quantified. Red arrowheads, BC-like lumina. Error bars indicate ± SEM (dot graphics) and ± SD (bar graphics). *, $P \leq 0.05$; **, $P \leq 0.01$; ***, $P \leq 0.001$.

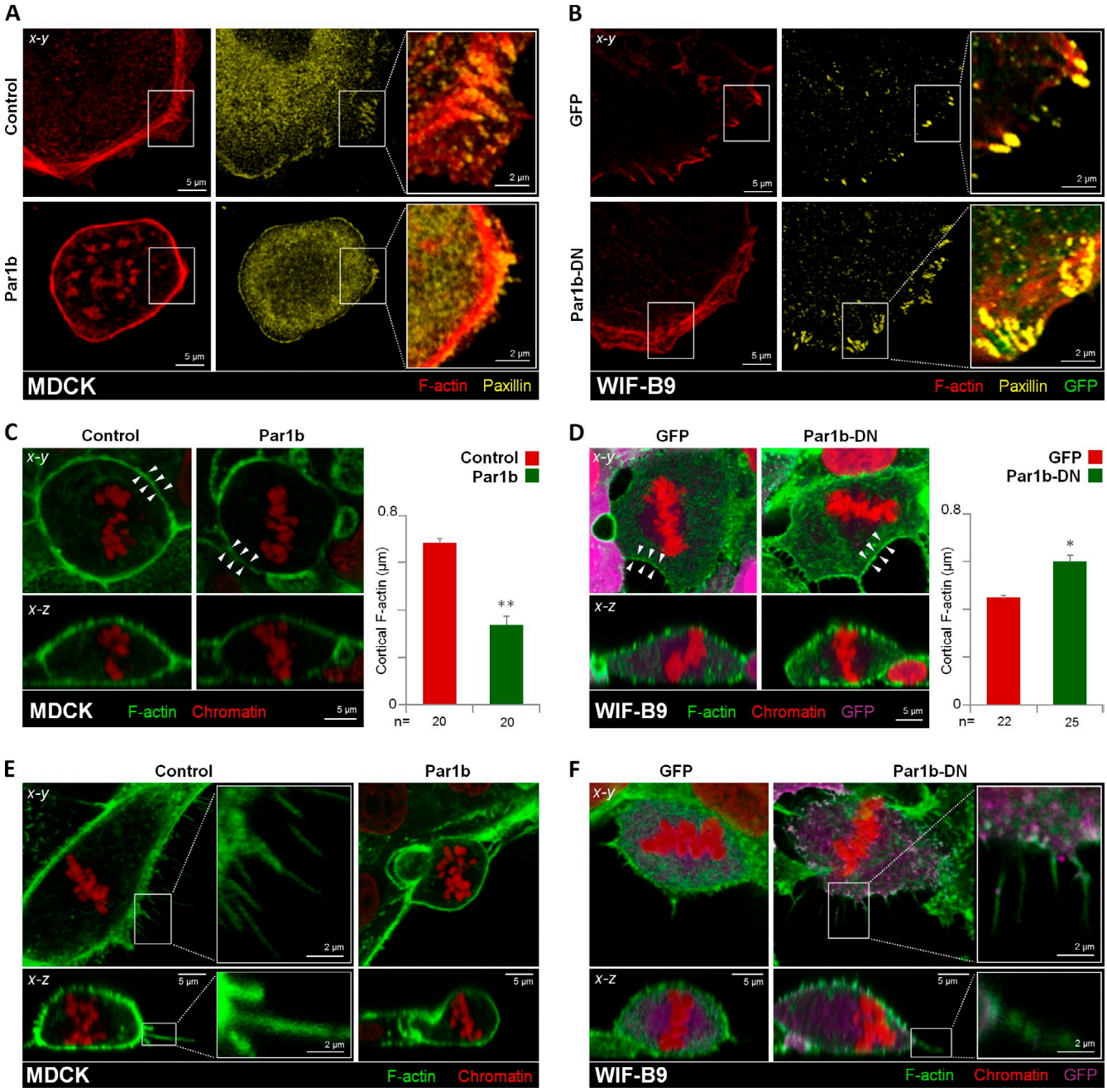

Figure S2. **Par1b overexpression in MDCK cells inhibits and Par1b depletion in WIF-B9 cells promotes focal adhesions and cortical F-actin.** Control and Par1b-MDCK cells (A, C, and E) or WIF-B9 control (GFP) and Par1b-depleted (Par1b-DN) cells (B, D, and F) were fixed and stained for F-actin (phalloidin-TRITC) and either focal adhesions (paxillin; A and B) or chromatin (C–F). The thickness of cortical F-actin (C and D, right panels) was determined as described in Materials and methods. White arrowheads, representative lumen-free regions of the cell cortex. Error bars indicate + SD. *, $P \leq 0.05$; **, $P \leq 0.01$.

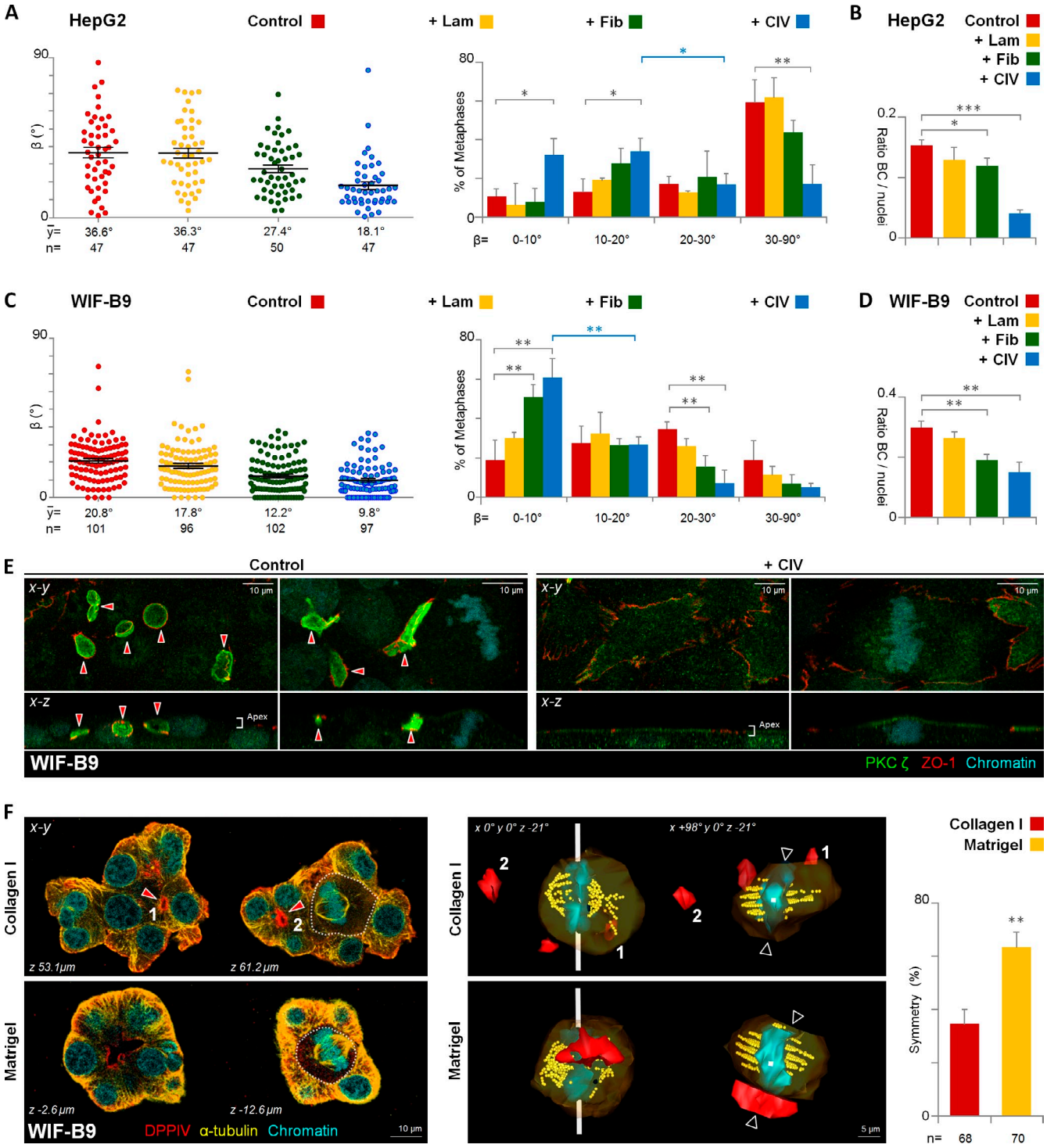

Figure S3. **Collagen IV promotes columnar polarity in HepG2 and WIF-B9 cells.** HepG2 (A and B) or WIF-B9 (C and D) cells were plated on either uncoated glass (Control), or on laminin- (+Lam), fibronectin (+ Fib), or collagen IV (+ CIV) matrices. Cells were fixed and stained for ezrin, α-tubulin, and chromatin (not depicted). The β angle (A and C) and the amount of BC-like lumina in interphase cells (B and D) were quantified. The shift from larger to smaller β-angles In the CIV samples was statistically significant for HepG2 cells with β angles in the 10–20° (33.9 ± 6.8%) category compared with the 20–30° (16.7 ± 5.9%) category and for WIF-B9 cells in the 0–10° (60.8 ± 9.7) vs. 10–20° (26.8 ± 3.8) category. (E) Localization of ZO-1 and the apical marker PKCζ/λ in WIF-B9 cells plated on glass or on collagen IV matrix. (F, left) 3D WIF-B9 cultures in either collagen I or Matrigel were fixed and stained for DPPIV, α-tubulin, and chromatin. (Middle) 3D models of the mitotic cells shown in the *x-y* sections of the left panel. (Right) The percentage of symmetric divisions in the cyst-like structures was quantified. Error bars indicate ± SEM (dot graphics) or + SD (bar graphics). *, P ≤ 0.05; **, P ≤ 0.01; ***, P ≤ 0.001.

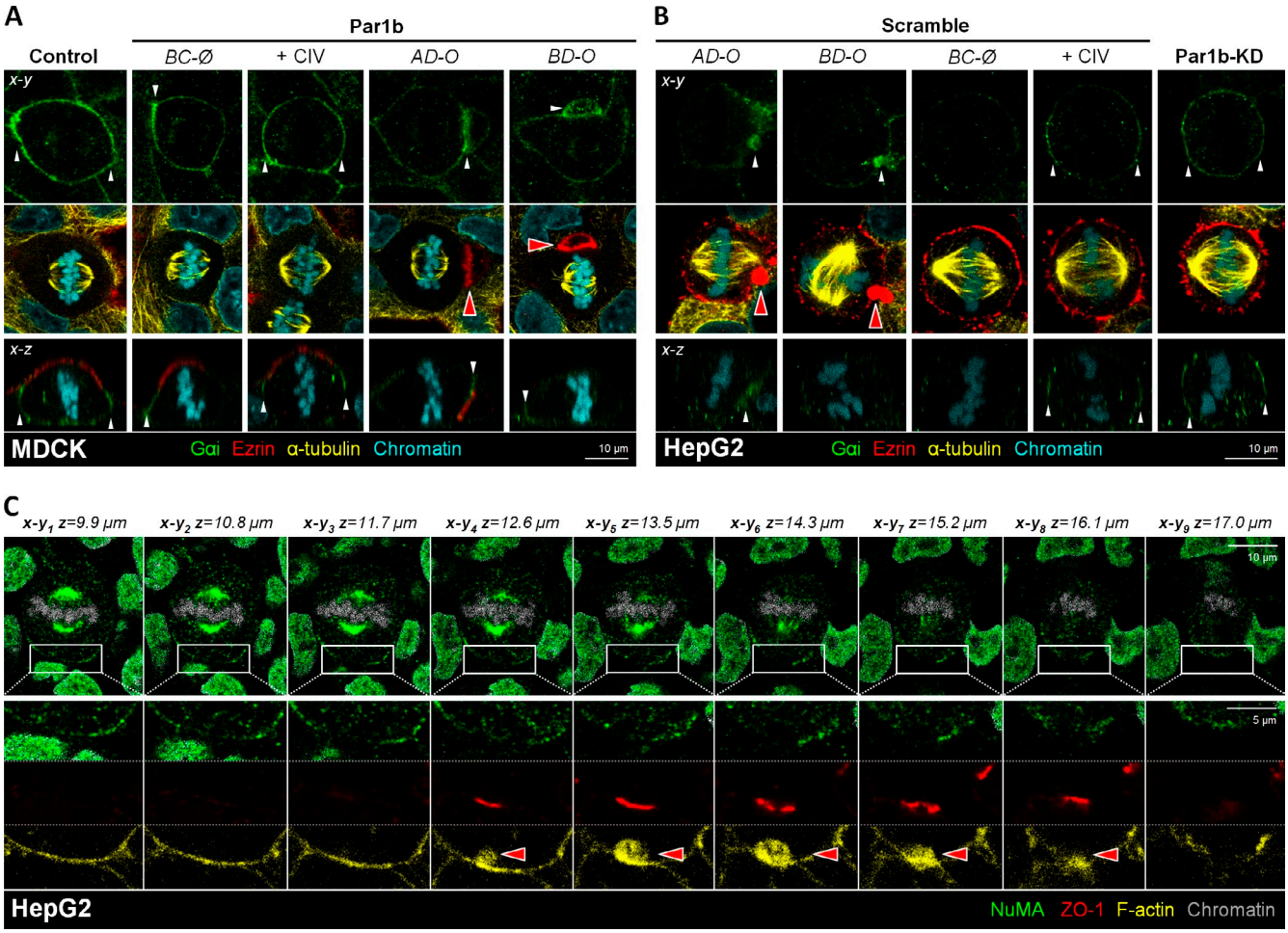

Figure S4. **NuMA is excluded from the lateral lumina of HepG2 cells, whereas Gαi is present at the lateral and luminal domains in MDCK-Par1b and HepG2 cells.** Control and Par1b expressing MDCK (A) or control (Scramble) and Par1b-depleted (Par1b-KD) HepG2 cells (B) were fixed and stained for Gαi, ezrin, α-tubulin, and chromatin. (C) Serial sections from a confocal stack of control HepG2 cells fixed and stained for NuMA, tight junctions (ZO-1), F-actin (phalloidin-TRITC), and chromatin (DAPI). Bottom panels represent enlarged areas of the dashed squares in the top panels. Note the exclusion of the NuMA protein from the area of the tight junctions and the F-actin–enriched lateral lumina (see schematics in Fig. 4 A for details regarding the nomenclature). Red arrowheads, BC-like lumina; white arrowheads, cortical enrichment of Gαi.

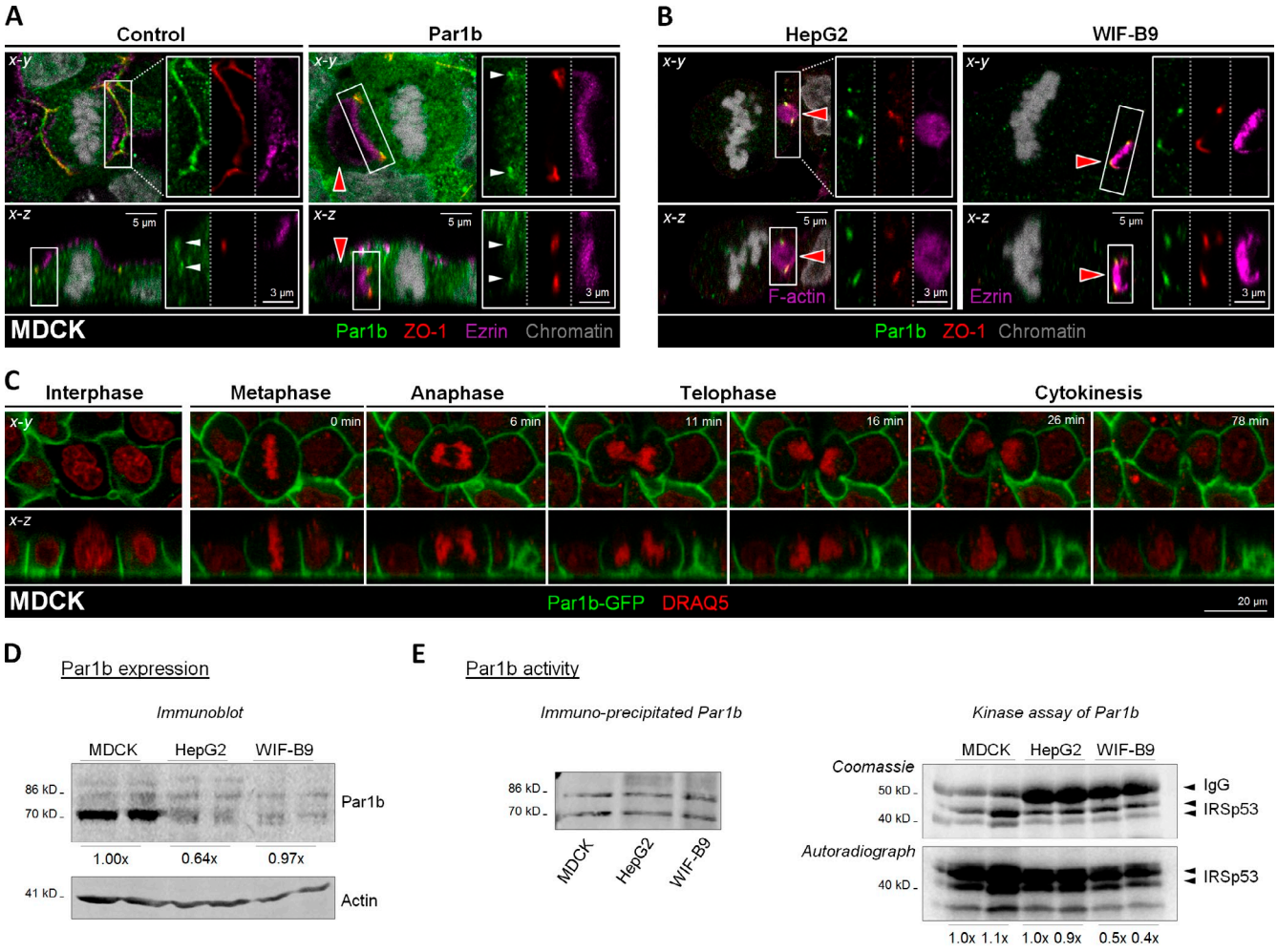

Figure S5. **Global Par1b activity in HepG2 and WIF-B9 cells is lower than that in MDCK cells, whereas Par1b localization during mitosis is similar in the three cell lines.** Control and Par1b expressing MDCK (A) or HepG2 and WIF-B9 cells (B) were fixed and stained for Par1b, ZO-1, chromatin, and ezrin or F-actin. The Par1b antibody was described in Cohen et al. (2004) and only labels Par1b at the tight junction region. (C) Time-lapse sequence in MDCK cells expressing Par1b-GFP co-stained with DRAQ5. Par1-GFP was not restricted to the tight junctions, but was present along the entire lateral domain as well as at the basal surface throughout all stages of mitosis. (D) Par1b immunoblot using a Par1b antibody raised against an epitope that is conserved in canine and human Par1b. Note that HepG2 and WIF-B9 cell lysates have about half the amount of Par1b compared with MDCK cell lysates. Actin was used as loading control. (E) Par1b activity in MDCK, HepG2, and WIF-B9 cells. (Left) Immunoblot of Par1b that was immunoprecipitated from the three cell lines, adjusted to equal Par1b protein levels, and then used for in vitro kinase assays. (Right) Coomassie stain and autoradiograph of the in vitro kinase assay using Par1b-IPs and IRSp53 as substrate. HepG2 Par1b shows comparable in vitro kinase activity to MDCK Par1b, whereas the kinase isolated from WIF-B9 cells is less active. The double band of Par1b in the blots represents two splice variants.

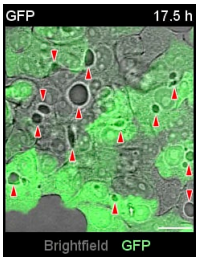

Video 1. **Lateral lumina formation in control and Par1b-depleted WIF-B9 cells.** Untransduced WIF-B9 cells (Control) and cells transduced with adenoviruses expressing either GFP-tagged dominant-negative Par1b (Par1b-DN) and the corresponding control (GFP) were recorded for 17.5 h at 0.5 h/frame in a confocal microscope (TCS SP5; Leica) using an 8,000-Hz resonant scanner. Red arrowheads, BC-like lumina. Bars, 10 µm.

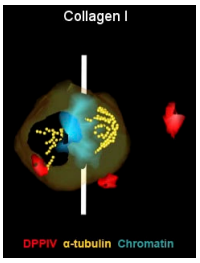

Video 2. **Metaphase plate orientation with respect to the lumen in WIF-B9 cells growing in cyst-like structures.** Confocal stacks (2 µm/section) obtained in a confocal microscope (TCS SP5; Leica) and their respective 3D models generated using IMOD software of a mitotic cell contained in the WIF-B9–derived cyst-like structures generated in collagen I or Matrigel. Bars, 10 µm.

Reference

Cohen, D., P.J. Brennwald, E. Rodriguez-Boulan, and A. Müsch. 2004. Mammalian PAR-1 determines epithelial lumen polarity by organizing the microtubule cytoskeleton. *J. Cell Biol.* 164:717–727. http://dx.doi.org/10.1083/jcb.200308104